# Magnetic microsphere-based mixers for microdroplets

Tamal Roy, Ashok Sinha, Sayan Chakraborty, Ranjan Ganguly, and Ishwar K. Puri

Citation: Physics of Fluids (1994-present) **21**, 027101 (2009); doi: 10.1063/1.3072602
View online: http://dx.doi.org/10.1063/1.3072602
View Table of Contents: http://scitation.aip.org/content/aip/journal/pof2/21/2?ver=pdfcov
Published by the AIP Publishing

# Magnetic microsphere-based mixers for microdroplets

Tamal Roy,[1] Ashok Sinha,[2] Sayan Chakraborty,[1] Ranjan Ganguly,[1,a)] and Ishwar K. Puri[2]
[1]*Department of Power Engineering, Jadavpur University, Kolkata 700098, India*
[2]*Department of Engineering Science and Mechanics, Virginia Polytechnic Institute and State University, Blacksburg, Virginia 24061, USA*

(Received 15 August 2008; accepted 12 December 2008; published online 10 February 2009)

While droplet-based microfluidic systems have several advantages over traditional flow-through devices, achieving adequate mixing between reagents inside droplet-based reactors remains challenging. We describe an active mixing approach based on the magnetic stirring of self-assembled chains of magnetic microspheres within the droplet as these stirrers experience a rotating magnetic field. We measure the mixing of a water-soluble dye in the droplet in terms of a dimensional mixing parameter as the field-rpm, fluid viscosity, and microsphere loading are parametrically varied. These show that the mixing rate has a maximum value at a critical Mason number that depends upon the operating conditions. © *2009 American Institute of Physics*.
[DOI: 10.1063/1.3072602]

## I. INTRODUCTION

Microfluidic devices that enable chemical reactions have a large number of sensor applications such as multistep chemical synthesis,[1] bioanalytical diagnostics,[2] DNA analysis,[3] catalytic hydrogenation of alkenes,[4] acid/base titrations,[5] etc. Recent advancements in microfabrication technology have led to the development of micrototal analytical systems ($\mu$-TAS),[6] more popularly known as *laboratory-on-a-chip* (LOC) devices. These devices have a relatively small size and are capable of performing the sample and reagent handling steps together with analytical measurements.[7]

Recent developments in producing and manipulating microdroplets in microfluidic environments have increased the use of droplet-based reactors for $\mu$-TAS applications.[8] Droplet-based microfluidic system offers an emerging LOC tool for the real-time online analysis of nanoliter biological and chemical agent volumes.[9,10] The droplets offer an easy means for compartmentalizing and isolating reactants, reduce the reagent consumption, and eliminate the possibility for cross-contamination due to dispersion, which is a major problem in a continuous flow microchannel. Thus, droplet-based microfluidic systems offer a promising platform for massively parallel DNA analysis and real-time molecular detection and recognition.[11–13] They also offer the promise of decoupling a binary yes/no response from the determination of agent concentration.[9]

Rapid mixing is essential in many microfluidic systems for proper biochemical analysis,[13] sequencing or synthesis of nucleic acids,[14] and for reproducible biological processes that involve cell activation,[15] enzyme reactions,[16] and protein folding.[17] However, at this small length scale, species transport in fluid flow is dominated by molecular diffusion, which is usually very slow in comparison with the flow residence time. This is particularly important for bioanalytical applications, since large organic molecules or biological cells have very low diffusivities.

A mixing process is termed active or passive, depending upon whether it requires supplementary energy input into the microscale flow (in addition to the pumping work). Passive devices achieve mixing in a relatively simple manner, e.g., through the use of channels that are fabricated based on elaborate mixing designs.[18,19] Chaotic micromixing can be induced by passing droplets through a meandering channel in an immiscible fluid.[20] Passive mixers are easier to integrate into LOC devices, but require relatively large path lengths and more complicated structures, and can have significantly lower mixing efficiencies than active systems.

Active devices have been based on rotating magnetic microbars that stir the flow,[21] acoustic cavitation cells,[22] electrokinetic instability,[23] periodic flow switching,[24] and pneumatically pumped rings.[25] Integration of these components into $\mu$-TAS devices is challenging, since they require electrical power and their mechanical construction within the device can be quite complex. These devices can therefore benefit from a simple "action-from-a-distance" solution that eliminates complexity and reduces the need to integrate a power supply and mechanical components into the microfabricated device. We discuss such a solution herein.

We use external magnetic fields to produce action from a distance at the microscale. The substances or reactants to be mixed are confined inside microliter-size droplets, effectively producing a self-contained mixer within the droplet. The droplets could rest on a substrate, be immersed in an immiscible buffer, or even be transported through a microchannel by an immiscible host fluid.[26] Mixing in the droplet is achieved by dispersing a measured quantity of magnetic microspheres in the droplet liquid and applying a rotating field.[27] The magnetic beads are 0.5–4 $\mu$m diameter polystyrene/silica beads impregnated with superparamagnetic iron oxide nanoparticles. The beads are commercially available in different sizes, composition, and properties.[28] Magnetic beads self-aggregate to form chains that rotate in

[a)]Author to whom correspondence should be addressed. Electronic mail: ranjan@pe.jusl.ac.in.

 

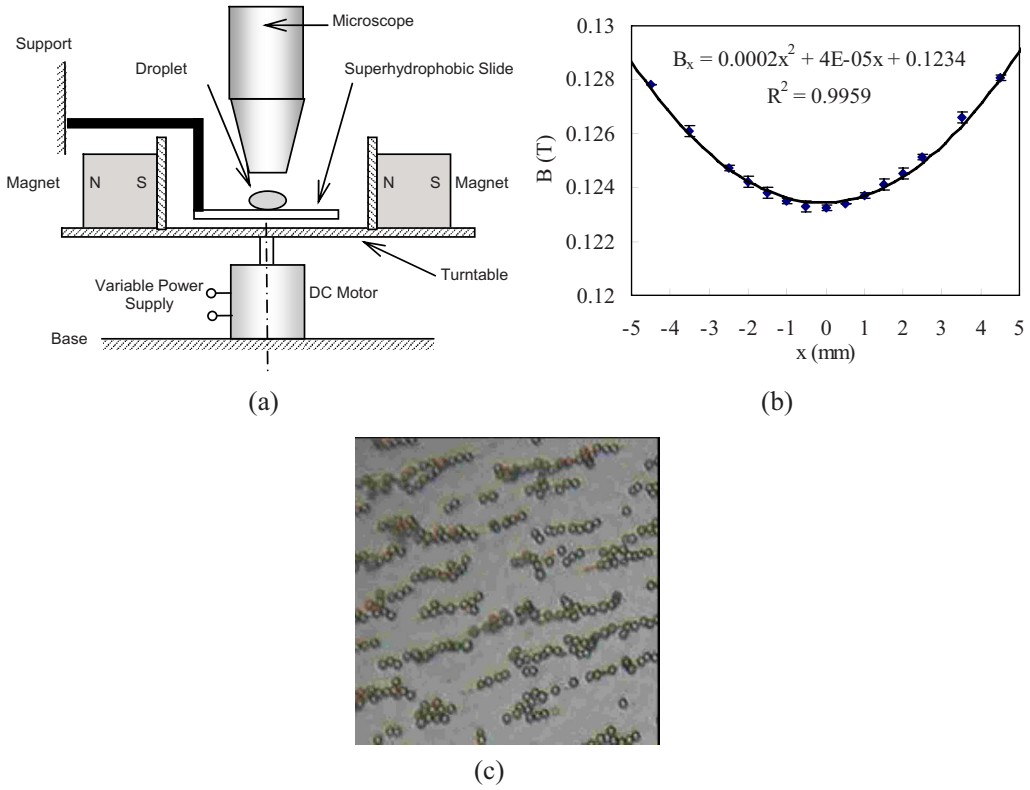


FIG. 1. (Color online) (a) Schematic of the experimental setup. (b) Variation of the magnetic field strength of the component perpendicular to the pole faces in the region between them. The field gradient is zero at the droplet location ($x$=0). (c) Self-assembly of magnetic microspheres into chains (500× image) under the influence of a homogeneous static magnetic field $B_0$=0.123 T.

synchronism with the field,[29,30] causing active mixing in the droplet.

Since the beads can be functionalized with a large variety of antibodies, they can also be used for quick and selective "tagging" biomolecules or cells[31] within the droplet-based mixer. After the mixing operation, the beads can be easily separated out using a magnetic field gradient.[32] Thus, bioanalytical diagnostics involving immunomagnetic separation can also be performed in such a droplet.

The field induced dynamic chain formation and rotation of magnetic microspheres due to a rotating magnetic field has been computationally investigated by several researchers using the particle dynamics,[30,33] direct numerical simulation,[34] and lattice Boltzmann methods.[35] Their results predicted that the mixing induced by rotating chains of magnetic microspheres depends on a dimensionless Mason number, which represents the ratio of the viscous torque to the magnetic torque. Although the structure of the predicted rotating magnetic chains has been adequately validated through experimental measurements,[30,35,36] the corresponding results for a quantitative evaluation of mixing are absent from literature. Therefore, we experimentally demonstrate the mixing enhancement in a microliter-size sessile droplet by rotating chains of magnetic microspheres and quantify the mixing rate in terms of the half-life of decay of a normalized mixing index. We investigate the influence of several operating parameters on the overall mixing rate, e.g., the rotational speed of the magnetic field, droplet liquid viscosity, and the magnetic particle concentration in the liquid.

## II. EXPERIMENTAL CONFIGURATION

The experimental configuration is schematically described in Fig. 1(a). A micro- or nanoliter volume water droplet, impregnated with a measured quantity of magnetic microspheres (CMAGPS 2.5 Corpuscular Inc., available in a dense suspension of 25 mg/ml) is deposited on a superhydrophobic substrate using a digital microdispenser. The magnetic beads are initially homogeneously suspended in the background liquid by shaking the suspension for 30 min in an ultrasonic bath (Misonix, 40 kHz) before dispensing. The polystyrene beads, containing magnetic nanoparticles, have a mean diameter of ~2.65 $\mu$m and a mean magnetization of 20 emu at 10 000 Oe. This corresponds to effective magnetic susceptibility of $\chi_{\text{eff}}$=0.019. The droplet-microsphere suspension is subjected to a magnetic field by placing it between two aligned NdFeB permanent magnets (residual magnetism of 1.2 T at the pole faces) that are mounted on a variable-speed turntable. The magnetic field intensity is measured by a Hall probe digital Gaussmeter (DGM 900, Ferrites India). All experiments are performed for magnetic field distribution shown in Fig. 1(b) for a base magnetic field of $B_0$ =0.123 T. As seen in that figure, the field gradient at the droplet location is nearly zero.

During an experiment, the droplets are first deposited on the superhydrophobic substrate, following which a chain-forming time of 10 s is allowed for the microspheres to form chainlike structure under the influence of the imposed magnetic field [as shown in Fig. 1(c)]. A dye is then injected into

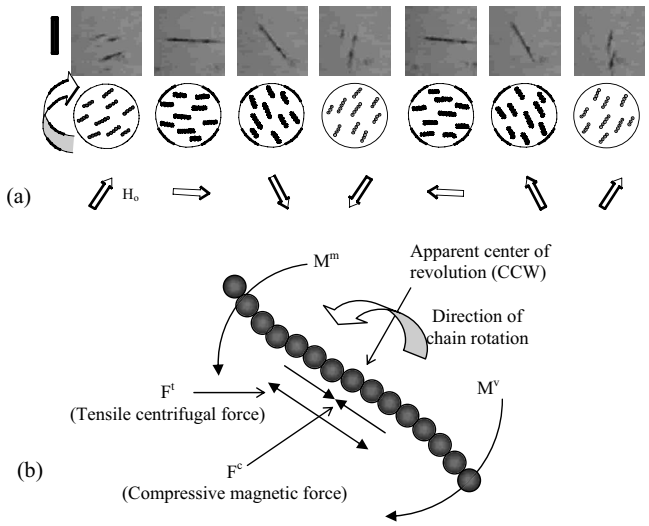


FIG. 2. (a) Rotation of the magnetoresponsive chains as the imposed magnetic field rotates at $\omega$=5 rpm. Here, the chains are used as localized rotors or stirrers. (The size of the scale on the left is 10 $\mu$m.) (b) Schematic showing the forces and moments acting on a particle chain, where $M^m$ denotes the driving magnetic moment and the reaction of the resistive moment $M^v$ favors the stirring action within the droplet.

the droplet using a hydrophobic needle and the turntable rotated about its axis at a specified angular speed, which produces the rotating magnetic field. Care is taken to isolate the droplet from the convection currents of the surrounding air so as to prevent shear-induced mixing inside the droplet. Images are obtained using a microscope-mounted digital camera (Olympus SP 350) at 25 frames/s. The microscope (Magnus MSZ-TR zoom stereo trinocular) has a 4×10× optical zoom, while the camera has a 3.5× optical zoom [an additional 10× objective is fitted when the chain structures shown in Figs. 1(c) and 2(a) are viewed]. The recorded movies are subsequently split into color bitmap (RGB) hue-intensity histograms and their pixel information is obtained by image processing (using Magnus Image Pro and MATLAB). To eliminate errors induced due to the noise and shadows in the image, the hue-intensity histogram of a base reference image is subtracted from all other images.

The extent of mixing (i.e., the homogeneity with which the dye is distributed across the droplet) is quantified through a mixing index parameter[21]

$$C' = \sqrt{(1/N)\sum_{1}^{N}[(P-\bar{P})^2/\bar{P}^2]}, \quad \text{for} \quad 0 \le P \le 256, \tag{1}$$

where the mean pixel value $\bar{P}=(1/N)\Sigma_i^N P$ and $N$ denotes the total number of pixels. Initially, when the dye is relatively unmixed, the variance of the pixel density is large, and $C'$ has a correspondingly large value $(C_0')$. As mixing progresses, the hue-intensity distribution becomes more uniform so that, for perfect mixing, the value of $C$ approaches a steady low value $(C_\infty')$. When the mixing index parameter is normalized as

$$C = \frac{(C' - C_\infty')}{(C_0' - C_\infty')}, \tag{2}$$

the $C$ versus $t$ curve varies from unity (unmixed state) to zero (fully mixed state).

Thus, $C(t)$ exhibits a typical exponential time decay that can be approximated as $C(t) \sim \exp(-t/\tau)$, where $\tau$ denotes the characteristic mixing time that is calculated from the hue-intensity histograms. We compare various magnetic chain induced mixing times with a case for purely diffusive mixing (i.e., when the magnetic field does not rotate). Parametric investigations reveal the influence of the rotational speed of the magnetic field (i.e., the rpm of the turntable), the viscosity of the droplet liquid (by premixing a measured amount of glycerol) and the particle number density.

## III. RESULTS AND DISCUSSION

### A. Behavior of the rotating chains

As soon as the substrate containing the droplet is placed in the magnetic field, the particles tend to form the chains [Fig. 1(c)] and when the magnetic field is rotated, these chains also follow its changing orientation [see Fig. 2(a)]. When this occurs, the chain containing $N$ spherical particles experiences a magnetic torque $M^m$ and an opposing viscous drag $M^v$ [as illustrated in Fig. 2(b)] such that[36,37]

$$M^m = \frac{\mu_0\mu_r}{4\pi}\frac{3|\vec{m}|^2N^2}{2(2a)^3}\sin(2\alpha), \quad \text{and}$$
$$M^v = \frac{4}{3}N\pi a^3\frac{2N^2}{\ln(N/2)}\eta\omega. \tag{3}$$

Here $\alpha$ denotes the angle between the rotating field and the magnetization vector $\vec{m}$ of a particle, $N$ the number of particles in a chain, $\mu_r$ the relative permeability of the medium, $\eta$ the fluid viscosity, and $\omega$ the angular velocity of the chains. Two other forces influence the chain integrity. The tensile force $F^t$ acting on the chain arises due to the centrifugal force on the rotating particles (which is negligibly small as compared to the magnetic and viscous forces for our experiments) promotes chain disintegration. The compressive force $F^c$ occurs due to the magnetic interaction between the particles and tends to hold the chain together. The response of a chain to the magnetic force is characterized through the Mason number[36]

$$\text{Ma} = \frac{\ln(N/2)}{N}\frac{M^v}{M^m}\sin(2\alpha) = \frac{\mu_0 32\omega\eta}{\mu_r\chi_{\text{eff}}^2|B_0^2|}, \tag{4}$$

which compares the magnitudes of the viscous and magnetic forces. When $B_0$=0.123 T, $\omega$=5 rpm, $\chi_{\text{eff}}$=0.019 and $\eta$ =0.0009 in water (i.e., $\mu_r \approx 1$) the particle chains in Fig. 2(a) correspond to Ma=0.003. For these conditions, the microspheres form long unbroken chains that are approximately 10–15 $\mu$m (i.e., 5–7 particles) long, which rotate in synchronism with the imposed magnetic field. The value of $\alpha$ for these chains is observed to be a very small angle, and so they closely follow the orientation of the imposed rotating magnetic field, as shown schematically in Fig. 2(a).

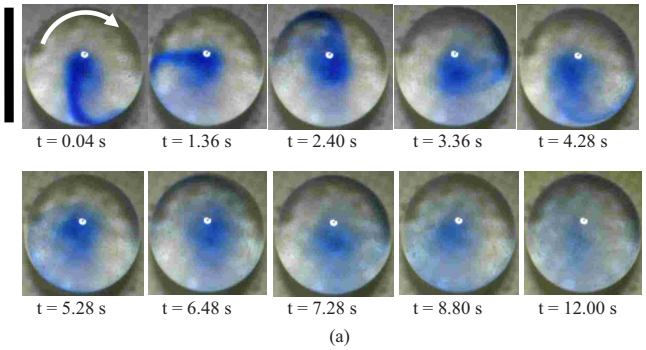


(a)

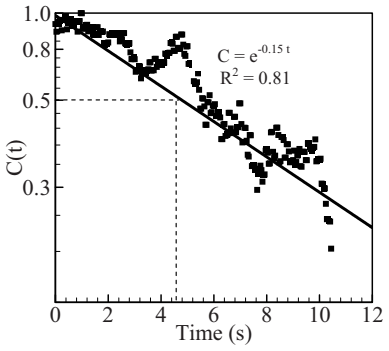


(b)

FIG. 3. (Color online) (a) Magnetically stirred mixing of a dye in the laboratory-in-a-droplet arrangement. (b) The corresponding variation of the mixing parameter $C$ with time shows a nearly exponential decay. The mixing half-life $t_{1/2}$ for this case is 4.6 s ($\eta=1.1\times10^{-3}$ Pa s, $\omega=180$ rpm). The white arrow denotes the direction of rotation and the vertical line a length scale of 1 mm.

### B. Quantification of mixing in the droplet

When a water-soluble blue dye is introduced into the droplet and spurious fluid motion in the droplet (due to the disturbances caused by ambient air currents) is suppressed, mixing of the dye occurs solely through molecular diffusion. However, when the droplet liquid is loaded with magnetic microspheres and a homogeneous rotating magnetic field is applied, rotating chains of magnetic microspheres lead to advective mixing within the droplet. Figure 3(a) shows a time sequence of images that illustrate the magnetically assisted mixing of a dye inside a 500 nl droplet containing a 10% (by volume) glycerol-in-water mixture (i.e., $\eta=1.1\times10^{-3}$ Pa s). When the mixing index is calculated as per Eqs. (1) and (2), the normalized $C$ vs $t$ curve shown in Fig. 3(b) is obtained.

The initial time $t=0$ denotes the instant when the injector is completely withdrawn after dye is injected into the droplet. In Fig. 3(a), the dye is observed in its most concentrated form at $t=0.04$ s. With time, as the droplet is rotated clockwise at $\omega=180$ rpm, the dye streak rotates in the same direction due to viscous interaction between the rotating chains and the liquid, and also stretches and diffuses into the host liquid. The stretching of the dye streak increases with time, which also enhances diffusion, leading to a nearly homogeneous final mixture at $t=12$ s. The initial variance of the hue intensity is large and $C\approx1$, but with progressive mixing in the droplet, its value decreases to zero according to the relation

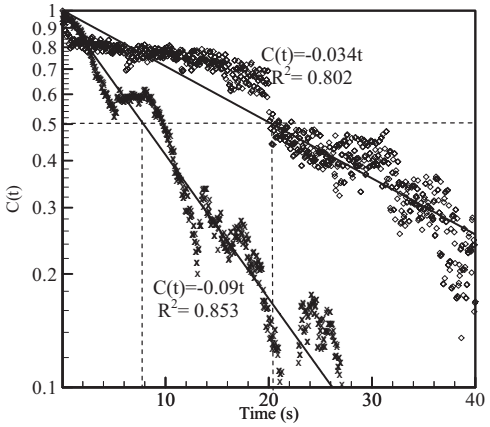


FIG. 4. The time variation of the mixing parameter $C$ and the mixing half-lives $t_{1/2}$ obtained from $C$-$t$ curves for $\eta=0.001\ 55$ Pa s. The dotted vertical lines indicate $t_{1/2}$ values with (7.9 s) and without (20.3 s) stirring.

$$C(t)=\exp(-0.15t). \tag{5}$$

The half-life of mixing $t_{1/2}$ is the time required to attain a value of $C=0.5$, i.e.,

$$t_{1/2}=0.6932/0.15=4.6\ \text{s}. \tag{6}$$

### C. Effect of $\omega$ and $\eta$ on mixing

Figure 4 presents the $C$ versus $t$ plots for two cases, one for the purely diffusive mixing ($\omega=0$) and the other with a rotating magnetic field ($\omega=180$ rpm) inside a 500 nl droplet containing a 20% (by vol.) glycerol-in-water water solution (for which $\eta=1.55\times10^{-3}$ Pa s). The value of $t_{1/2}=20.3$ s for the purely diffusive case, and 7.9 s, i.e., 2.6 times faster, when the field is rotated. Both droplets are produced from the same initial mixture that has a magnetic microsphere concentration of 1.0 mg/ml.

Comparing Figs. 3(b) and 4 shows that when $\omega=180$ rpm, the value of $t_{1/2}$ increases from 4.6 s to 7.9 s as the liquid viscosity increases from $\eta=1.1\times10^{-3}$ to $1.55\times10^{-3}$ Pa s. This difference is attributed to several competing factors. While a higher liquid viscosity enhances the momentum exchange between the rotating chains and the droplet fluid, which is favorable for mixing, it also leads to greater viscous dissipation within the droplet (and consequently a larger momentum transfer to the narrow base where the droplet is attached to the superhydrophobic surface), which dominates and reduces the mixing rate.

Figure 5(a) presents the variation of $t_{1/2}$ when $\omega$ and $\eta$ are varied. For pure water ($\eta=0.902\times10^{-3}$ Pa s), the mixing half-life decreases from 17.3 s for purely diffusive mixing to 1.7 s at $\omega\approx210$ rpm as per the relation

$$t_{1/2}=c_0+c_1\omega+c_2\omega^2 \tag{7}$$

(where $c_0$, $c_1$, and $c_2$ are constants). The fastest mixing occurs when

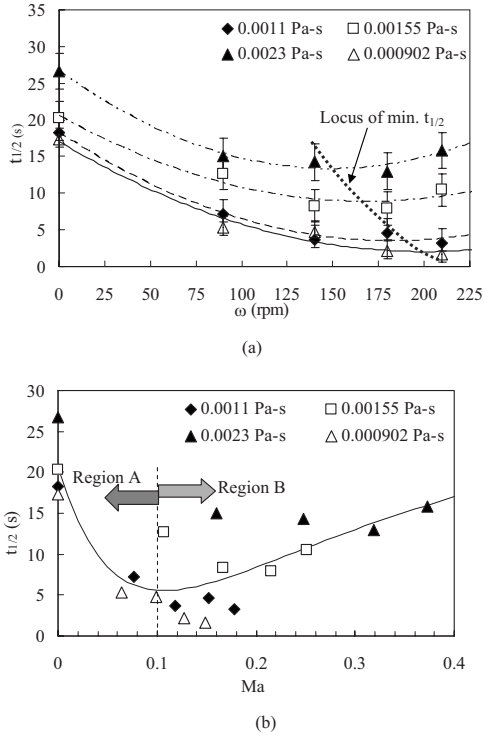


FIG. 5. (a) Variation of $t_{1/2}$ with the field rotational speed for different viscosities of the droplet liquid when the glycerol content in the solution is varied by volume. The mixing half-life attains a minimum value at a critical rpm, beyond which it increases again. The error bars represent the variance of $t_{1/2}$ obtained from ten readings for each operating condition. (b) The same data presented vs Ma.

$$\omega_{\text{crit}} = -\tfrac{1}{2}(c_1/c_2). \tag{8}$$

Similar observations are made for at higher liquid viscosities ($\eta = 1.1\times10^{-3}$, $1.55\times10^{-3}$ and $2.3\times10^{-3}$ Pa s) and, as discussed above, the $t_{1/2}$ versus $\omega$ curves shift upward with increasing $\eta$. The values of $c_0$, $c_1$, and $c_2$ are provided in Table I.

Increasing $\omega$ provides two competing effects on mixing. While it increases momentum transfer between the fluid and the chains, at high enough values of $\omega$ (and $\eta$) the chains buckle due to magnetic drag on the particles at the periphery of a chain, and chain breakdown occurs for large enough values of $\omega$.[37] The maximum number $N_{\text{max}}$ of beads that can be part of a chain decreases as either $\omega$ or $\eta$ is increased so that $N_{\text{max}} \propto \text{Ma}^{-1/2}$.[30] As the effective chain length is reduced due to buckling and breakdown, the overall viscous interaction between the chains and the liquid also decreases. Thus, $t_{1/2}$ should first decrease until chain breakdown is initiated

TABLE I. List of the curve-fit constants for Eq. (7).

| $\eta$ ($\times10^3$ Pa s) | $c_0$ | $c_1$ | $c_2$ ($\times10^4$) |
|---|---|---|---|
| 0.902 | 17.08 | −0.1503 | 3.76 |
| 1.1 | 18.24 | −0.1628 | 4.33 |
| 1.55 | 20.57 | −0.1392 | 4.01 |
| 2.3 | 26.62 | −0.1786 | 5.99 |

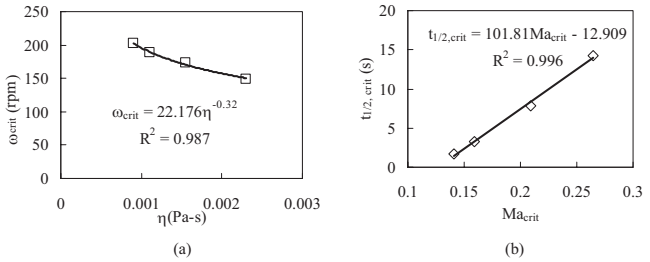


FIG. 6. (a) Variation of the critical rpm as the droplet liquid viscosity is altered. (b) Variation of the corresponding critical half-life of mixing as a function of $\text{Ma}_{\text{crit}}$.

and then increase with increasing $\omega$. The constants $c_0$, $c_1$, and $c_2$ of Eq. (7) are obtained from polynomial curve fits of the data presented in Fig. 5(a). Here, $c_0$ denotes the mixing time with pure diffusion ($\omega=0$), $c_1$ is negative (see Table I), since an increase in the advective velocity leads to a reduction in the mixing time, and $c_2$ accounts for the effect of chain breakdown. The value of $c_2$ is influenced by several factors such as the particle-particle interaction (magnetic attraction, steric repulsion, and friction) and the viscous force. The second term in Eq. (7) is proportional to $\omega$ and therefore denotes the influence of the advective velocity.

The $t_{1/2}$ versus Ma plots in Fig. 5(b) illustrate the competing effects of $\omega$ and $\eta$ and follow the general relation that is obtained through a rational curve fit,

$$t_{1/2} = (41.97\ \text{Ma}^2 - 6.602\ \text{Ma} + 0.5705)/(\text{Ma}^2 + 0.2143\ \text{Ma} + 0.0276). \tag{9}$$

The mixing half-life initially decreases with increasing Ma to assume a minimum near Ma=0.1, and then increases as the value Ma increases. Similar results have been reported by Calhoun *et al.*[35] who determined a critical Ma=0.12 through LB simulations, and Kang *et al.*[34] who, through a direct numerical method, also established an optimum Ma=0.002 (equivalent to Ma=0.06 as per our definition), which they correlated with the occurrence of rotating and corotating flows caused by alternating chain breakup and reformations that lead to the fastest mixing. In region A of Fig. 5(b), mixing is limited by the extent of momentum transfer, while in region B, it is limited by chain deformation and breakdown.

The location of $t_{1/2}$ minima in Fig. 5(a) is found to shift toward decreasing $\omega$ as $\eta$ increases, which is shown by the dotted line. The minimum value of $t_{1/2}$ occurs at $\omega \approx 210$ rpm for pure water, while for a 30% glycerol-water mixture (i.e., $\eta = 2.3\times10^{-3}$ Pa s), it occurs at $\omega \approx 140$ rpm. Figure 6(a) presents a corresponding plot of $\omega_{\text{crit}}$ as a function of $\eta$, which scales as $\omega_{\text{crit}} \propto \eta^{-0.32}$. For specified values of $\chi_{\text{eff}}$ and $B_0$, $\text{Ma} \propto \omega\eta$, and the critical Mason number exhibits a weak dependence on the fluid viscosity as $\text{Ma}_{\text{crit}} \propto \eta^{0.68}$. The $t_{1/2}$ minima values (at the $\omega_{\text{crit}}$ conditions) exhibit a linear relationship with respect to $\text{Ma}_{\text{crit}}$, as shown in Fig. 6(b). Thus, while Fig. 5(b) illustrates whether the mixing within the droplet is limited by momentum transfer or by

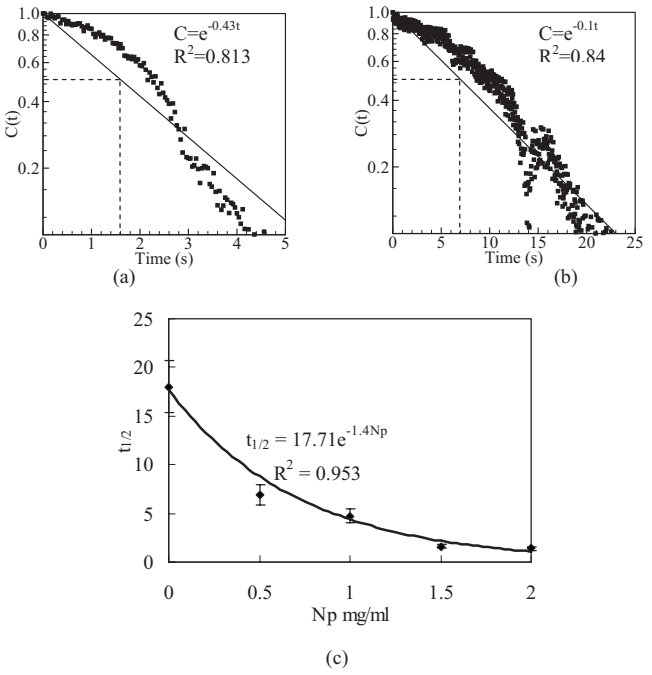


FIG. 7. $C$ vs $t$ plots for particle loadings of (a) 1.5 mg/ml and (b) 0.5 mg/ml. The magnetic field is rotated at $\omega=140$ rpm in pure water. Half-lives for mixing are 1.6 s for (a) and 6.9 s for (b). (c) Variation of $t_{1/2}$ with $N_p$. The error bars represent the variance of $t_{1/2}$ obtained from ten readings for each operating condition.

chain breakdown over a wide range of Mason numbers, Fig. 6 shows how the optimum mixing condition varies with changing fluid viscosity.

### D. Effect of particle loading on mixing

The advective motion in the droplet depends on the relative number of particle chains contained in a unit volume of the droplet liquid, which is a function of the particle loading $N_p$. Figures 7(a) and 7(b) present the $C$ versus $t$ relationships for mixing in pure water (i.e., $\eta=0.902\times10^{-3}$ Pa s) at $\omega=140$ rpm with a dense (1.5 mg/ml) and a dilute (0.5 mg/ml) particle loadings, respectively. The value of $t_{1/2}$ for the former case is 1.6 s, while that for the latter is 6.9 s. Therefore, a threefold increase in particle loading improves mixing by a factor of 4.3. An increase in particle loading can influence chain formation in two ways. First, enhancing the particle concentration promotes chain formation and growth during the initial incubation period. Second, it also leads to formation of a larger number of chains. Both factors enhance mixing as shown in Fig. 7(c). The $t_{1/2}$ values decrease significantly from 17.7 to 1.6 s as $N_p$ increases from 0 to 1.5 mg/ml, and then marginally as it is increased to 2.0 mg/ml. Higher particle loadings produced dark rotating chain images, which were difficult to reliably analyze.

## IV. CONCLUSIONS

We demonstrate a novel approach to enhance mixing in micron-sized droplets through magnetic stirring. Magnetic microspheres, which are added to the droplet form aligned chains *in situ* under the influence of a homogeneous magnetic field. When the magnetic field is rotated, the chains also rotate synchronously. Viscous interactions between the particle chains and the liquid induce adjective motion inside the droplet thereby enhancing mixing, which is otherwise diffusion limited. The mixing of a dye is characterized through a dimensionless mixing parameter that decays from unity (denoting an unmixed state) to zero (denoting a completely mixed state). The influence of other parameters, e.g., the field rpm, fluid viscosity and the microsphere number density, on the half-life of decay for the mixing parameters is also experimentally determined.

For a specified fluid viscosity, the mixing half-life initially decreases as the field rpm is increased, but then increases at higher rotational speeds. For a fixed field rpm, the mixing half-life increases monotonically with the viscosity of the droplet liquid. The mixing rate increases with the Mason number when $\mathrm{Ma}<0.1$, while for greater $M$ values it decreases. The value of $\mathrm{Ma}_{\mathrm{crit}}$ has a weak dependence on the fluid viscosity and the critical value of the mixing half-life varies linearly with $\mathrm{Ma}_{\mathrm{crit}}$. The mixing rate increases monotonically with particle loading, but this improvement diminishes at higher particle loadings.

## ACKNOWLEDGMENTS

The corresponding author gratefully acknowledges the support of the Department of Science and Technology, India, for supporting this work under its SERC Fast Track Project for Young Scientists Scheme, Grant No. SR/FTP/ETA-07/2006.

[1] G. H. Seong and R. M. Crooks, "Efficient mixing and reactions within microfluidic channels using microbead-supported catalysts," J. Am. Chem. Soc. **124**, 13360 (2002).
[2] H. Chou, C. Spence, A. Scherer, and S. R. Quake, "A microfabricated device for sizing and sorting DNA molecules," Proc. Natl. Acad. Sci. U.S.A. **96**, 11 (1999).
[3] M. A. Burns, B. N. Johnson, S. N. Brahmasandra, K. Handique, J. R. Webster, M. Krishnan, T. S. Sammarco, P. M. Man, D. Jones, D. Heldsinger, C. H. Mastrangelo, and D. T. Burke, "An integrated nanoliter DNA analysis device," Science **282**, 484 (1998).
[4] M. W. Losey, R. J. Jackman, S. L. Firebaugh, M. A. Schmidt, and K. F. Jensen, "Design and fabrication of microfluidic devices for multiphase mixing and reaction," J. Microelectromech. Syst. **11**, 709 (2002).
[5] J. R. Burns and C. Ramshaw, "The intensification of rapid reactions in multiphase systems using slug flow in capillaries," Lab Chip **1**, 10 (2001).
[6] A. Manz, N. Graber, and H. M. Widmer, "Miniaturized total chemical analysis systems: A novel concept for chemical sensing," Sens. Actuators B **1**, 244 (1990).
[7] P. A. Greenwood and G. M. Greenway, "Sample manipulation in micro total analytical systems," Trends Analyt. Chem. **21**, 726 (2002).
[8] A. Huebner, S. Sharma, M. Srisa-Art, F. Hollfelder, J. B. Edel, and A. J. deMello, "Microdroplet: A sea of applications?" Lab Chip **8**, 1244 (2008).
[9] F. Su, S. Ozev, and K. Chakrabarty, "Ensuring the operational health of droplet-based microelectrofluidic biosensor systems," IEEE Sens. J. **5**, 763 (2005).
[10] I. Barbulovic-Nad, H. Yang, P. S. Park, and A. R. Wheeler, "Digital microfluidics for cell-based assays," Lab Chip **8**, 519 (2008).
[11] V. Srinivasan, V. K. Pamula, and R. B. Fair, "An integrated digital microfluidic lab-on-a-chip for clinical diagnostics on human physiological fluids," Lab Chip **4**, 310 (2004).
[12] Y.-J. Liu, D.-J. Yao, H.-C. Lin, W.-Y. Chang, and H.-Y. Chang, "DNA ligation of ultramicro volume using an EWOD microfluidic system with coplanar electrodes," J. Micromech. Microeng. **18**, 045017 (2008).

[13]K. A. Shaikh, K. S. Ryu, E. D. Goluch, J. M. Nam, J. W. Liu, S. Thaxton, T. N. Chiesl, A. E. Barron, Y. Lu, C. A. Mirkin, and C. Liu, "A modular microfluidic architecture for integrated biochemical analysis," Proc. Natl. Acad. Sci. U.S.A. **102**, 9745 (2005).
[14]P. A. Auroux, D. Iossifidis, D. R. Reyes, and A. Manz, "Micro total analysis systems. 2. Analytical standard operations and applications," Anal. Chem. **74**, 2637 (2002).
[15]C. Ionescu-Zanetti, R. M. Shaw, J. G. Seo, Y. N. Jan, L. Y. Jan, and L. P. Lee, "Mammalian electrophysiology on a microfluidic platform," Proc. Natl. Acad. Sci. U.S.A. **102**, 9112 (2005).
[16]C. K. Fredrickson and Z. H. Fan, "Macro-to-micro interfaces for microfluidic devices," Lab Chip **4**, 526 (2004).
[17]D. E. Hertzog, X. Michalet, M. Jäger, X. Kong, J. G. Santiago, S. Weiss, and O. Bakajin, "Femtomole mixer for microsecond kinetic studies of protein folding," Anal. Chem. **76**, 7169 (2004).
[18]P. J. A. Kenis, R. F. Ismagilov, and G. M. Whitesides, "Microfabrication inside capillaries using multiphase laminar flow patterning," Science **285**, 83 (1999).
[19]A. D. Stroock, S. K. W. Dertinger, A. Ajdari, I. Mezić, H. A. Stone, and G. M. Whitesides, "Chaotic mixer for microchannels," Science **295**, 647 (2002).
[20]H. Song, D. Tice, and R. F. Ismagilov, "A microfluidic system for controlling reaction networks in time," Angew. Chem., Int. Ed. **42**, 767 (2003).
[21]L.-H. Lu, K. S. Ryu, and C. Liu, "A magnetic microstirrer and array for microfluidic mixing," J. Microelectromech. Syst. **11**, 462 (2002).
[22]R. H. Liu, R. Lenigk, R. L. Druyor-Sanchez, J. N. Yang, and P. Grodzinski, "Hybridization enhancement using cavitation microstreaming," Anal. Chem. **75**, 1911 (2003).
[23]M. H. Oddy, J. G. Santiago, and J. C. Mikkelsen, "Electrokinetic instability micromixing," Anal. Chem. **73**, 5822 (2001).
[24]I. Glasgow and N. Aubry, "Enhancement of microfluidic mixing using time pulsing," Lab Chip **3**, 114 (2003).
[25]T. Thorsen, S. J. Maerkl, and S. R. Quake, "Microfluidic large-scale integration," Science **298**, 580 (2002).
[26]I. Shestopalov, J. D. Tice, and R. F. Ismagilov, "Multi-step synthesis of nanoparticles performed on millisecond time scale in a microfluidic droplet-based system," Lab Chip **4**, 316 (2004).
[27]R. Ganguly and I. K. Puri, "Field-assisted self-assembly of superparamagnetic nanoparticles for biomedical, MEMS and BioMEMS applications," Adv. Appl. Mech. **41**, 293 (2007).
[28]U. Häfeli, M. A. Lobedann, J. Steingroewer, L. R. Moore, and J. Riffle, "Optical method for measurement of magnetophoretic mobility of individual magnetic microspheres in defined magnetic field," J. Magn. Magn. Mater. **293**, 224 (2005).
[29]A. K. Vuppu, A. A. Garcia, and M. A. Hayes, "Videomicroscopy characterization of dynamically aggregated paramagnetic microrotors in an applied rotating magnetic field," Langmuir **19**, 8646 (2003).
[30]I. Petousis, E. Homburg, R. Derks, and A. Dietzel, "Transient behaviour of magnetic micro-bead chains rotating in a fluid by external fields," Lab Chip **7**, 1746 (2007).
[31]M. A. M. Gijs, "Magnetic bead handling on-chip: New opportunities for analytical applications," Microfluid. Nanofluid. **1**, 22 (2004).
[32]Y. Wang, Y. Zhao, and S. K. Cho, "Efficient in-droplet separation of magnetic particles for digital microfluidics," J. Micromech. Microeng. **17**, 2148 (2007).
[33]S. Melle, O. G. Calderón, G. G. Fuller, M. A. Rubio, "Microstructure evolution in magnetorheological suspensions governed by Mason number," Phys. Rev. E **68**, 041503 (2003).
[34]T. G. Kang, M. A. Hulsen, J. M. J. den Toonder, P. D. Anderson, and H. E. H. Meijer, "Chaotic mixing induced by a magnetic chain in a rotating magnetic field," Phys. Rev. E **76**, 066303 (2007).
[35]R. Calhoun, A. Yadav, P. Phelan, A. Vuppu, A. Garcia, and M. Hayes, "Paramagnetic particles and mixing in micro-scale flows," Lab Chip **6**, 247 (2006).
[36]S. L. Biswal and A. P. Gast, "Rotational dynamics of semiflexible paramagnetic particle chains," Phys. Rev. E **69**, 041406 (2004).
[37]S. L. Biswal and A. P. Gast, "Dynamics of an active magnetic particle in a rotating magnetic field," Anal. Chem. **76**, 6448 (2004).